Analysis of Oxidative Titrations of *Desulfovibrio gigas* Hydrogenase; Implications for the Catalytic Mechanism†

Lee Melvin Roberts and Paul A. Lindahl*

Department of Chemistry, Texas A&M University, College Station, Texas 77843

Received June 13, 1994; Revised Manuscript Received September 6, 1994⊗

ABSTRACT: The oxidative titrations of hydrogenase (Hase) from *Desulfovibrio gigas* [Barondeau, D. P., Roberts, L. M., & Lindahl, P. A. (1994) *J. Am. Chem. Soc. 116*, 3442] were simulated using model descriptions of the redox reactions in the enzyme. The data fit best to a model that assumed Hase contains one $[Fe_3S_4]^{1+/0}$ cluster, two $[Fe_4S_4]^{2+/1+}$ clusters, and a Ni center stable in four redox states (Ni-B, Ni-SI, Ni-C, and Ni-R), each separated by one electron. A model in which Ni-SI, Ni-C, and Ni-R correspond to Nickel(2+) dithiolate, nickel(1+) dithiol, and nickel(2+) dithiol hydride, respectively, is compatible with all established relevant properties of the Ni center. This model and the concept of redox microstates were employed to define electronic states of the enzyme and to reformulate the catalytic mechanism initially proposed by Cammack et al. [Cammack, R., Patil, D. S., Hatchikian, E. C., & Fernandez, V. M. (1987) *Biochim. Biophys. Acta 912*, 98] into three interconnected catalytic cycles. These cycles differ in the average oxidation level of the Fe_4S_4 clusters. The cycle with the most reduced clusters appears to operate reversibly (catalyzing both H_2 oxidation and H^+ reduction), while those with more oxidized clusters function only to oxidize H_2. The difference in reversibility is explained by assuming that Ni-R prefers to reduce an $[Fe_4S_4]^{2+}$ cluster instead of H^+ and that H^+ is reduced only when that Fe_4S_4 cluster is in its reduced state.

The nickel−iron hydrogenase from *Desulfovibrio gigas* (Hase[1]) contains four redox centers, including one $[Fe_3S_4]^{1+/0}$ cluster, two $[Fe_4S_4]^{2+/1+}$ clusters, and one mononuclear nickel complex (Moura et al., 1988; Cammack et al., 1988). The oxidized $[Fe_3S_4]^{1+}$ cluster exhibits an EPR signal at $g = 2.02$ and is reducible by one electron (Teixeira et al., 1983). The two $[Fe_4S_4]^{2+/1+}$ clusters, designated Fe_{4a} and Fe_{4b}, undergo one-electron redox chemistry (Teixeira et al., 1989). The reduced forms of these clusters exhibit broad, poorly understood EPR features rather than signals typical of other $[Fe_4S_4]^{1+}$ clusters having $S = 1/2$ or $S = 3/2$ system spin states (Cammack et al., 1987; Teixeira et al., 1989).

The Ni ion appears to be coordinated by at least two cysteine and one histidine ligands (Voordouw, 1992), possibly in a distorted octahedral or trigonal bipyramidal geometry (Eidsness et al., 1988; Kruger & Holm, 1990; Baidya et al., 1992a,b; Shoner et al., 1994). It can exist in four magnetic states known as Ni-AB, Ni-SI, Ni-C, and Ni-R (Teixeira et al., 1985; Bagyinka et al., 1993). Ni-AB is obtained when the enzyme is oxidized, and it almost certainly corresponds to Ni^{3+} (Moura et al., 1988). This state yields the Ni-A and/or the Ni-B EPR signals. Reduction of Ni-A yields Ni-SI, the EPR-silent intermediate state that probably corresponds to Ni^{2+}. Ni-SI is reduced to the EPR-active Ni-C state, and Ni-C is reduced to the fully reduced EPR-silent Ni-R state.

Since Ni-C arises by reducing the Ni^{2+}-containing enzyme, yields an EPR signal, and is associated with a photolabile hydrogenic species (either H^+, H^-, or H_2) (van der Zwaan et al., 1985; Whitehead et al., 1993), it has been designated as the following: (i) a protonated Ni^{1+} complex (Cammack et al., 1987); (ii) a Ni^{3+} hydride (Teixeira et al., 1989); (iii) a Ni^{3+} molecular hydrogen complex (Crabtree, 1986); (iv) a redox-inactive Ni^{2+} coupled to redox-active ligands or neighboring groups (Bagyinka et al., 1993); (v) a Ni^{1+} hydride (Baidya et al., 1992a); and (vi) a Ni^{1+} molecular hydrogen complex (van der Zwaan et al., 1987). Before the association with a hydrogenic species was established, Ni-C was also thought to arise from a Ni^{3+} complex (Kojima et al., 1983; Teixeira et al., 1985). The Ni-R state has been proposed to arise from Ni^0 (van der Zwaan et al., 1985), Ni^{2+} hydride (Cammack et al., 1987), and $Ni^{2+}(\eta^2\text{-}H_2)$ (Huang et al., 1993).

Hase is thought to cleave H_2 heterolytically (Krasna & Rittenberg, 1954), and the evidence for a hydrogenic species on the Ni center implicates this center as the active site. Cammack et al. (1987) proposed that active enzyme oxidizes H_2 as follows: Ni-SI (Ni^{2+}) reacts with H_2, forming Ni-R (Ni^{2+}-H^-) and a proton; Ni-R oxidizes by one electron, forming Ni-C (Ni^{1+}-H^+); and then Ni-C oxidizes by one electron, forming Ni-SI (Ni^{2+}) and another proton. One

† This work was supported by the Robert A. Welch Foundation (A-1170).

* Author to whom correspondence should be addressed.

⊗ Abstract published in *Advance ACS Abstracts,* November 1, 1994.

[1] Abbreviations: Hase, hydrogenase; EPR, electron paramagnetic resonance; ENDOR, electron−nuclear double resonance; XAS, X-ray absorption spectroscopy; E_m', midpoint potential at pH 8 (unless otherwise mentioned); ZED, zero-electron-difference Model; TED, two-electron-difference Model; FED, four-electron-difference Model; ZED_P, TED_P, and FED_P, models in which only EPR-active Ni ions are assumed to be redox-active; ZED_T, TED_T, and FED_T, models in which all Ni ions in the enzyme are assumed to be redox-active; Ni-A, the state of the Ni center exhibiting an EPR signal with $g_1 = 2.31$, $g_2 = 2.23$, $g_3 = 2.02$; Ni-B, the state exhibiting a signal with $g_1 = 2.33$, $g_2 = 2.16$, $g_3 = 2.02$; Ni-AB, the Ni-A and Ni-B states considered as one; Ni-SI, the EPR-silent state of the Ni center more reduced than Ni-AB and more oxidized than Ni-C; Ni-C, the state of the Ni center exhibiting an EPR signal with $g_1 = 2.19$, $g_2 = 2.16$, $g_3 = 2.02$; Ni-R, the EPR-silent state that is more reduced than Ni-C.

0006-2960/94/0433-14339$04.50/0

Fe_4S_4 cluster receives the electrons from the Ni center and transfers them, one at a time, to the other Fe_4S_4 cluster. This second cluster transfers the electrons to external electron acceptors, also one at a time. The role of the $[Fe_3S_4]^{1+/0}$ cluster in catalysis is unknown. Variations on this mechanism have been proposed. That proposed by Teixeira et al. (1989) includes a Ni^{3+}-H^- designation of Ni-C. Huang et al. (1993) proposed that Ni-R is a $Ni^{2+}(\eta^2$-$H_2)$, and Kovacs (1993) and Shoner et al. (1994) proposed that H_2 adds across a Ni^{2+}−SR bond of Ni-SI, affording Ni^{2+}-H^-(RSH) for Ni-R.

We recently performed four stoichiometric oxidative titrations of Hase, starting in the Ni-C state and ending with Ni-B (Barondeau et al., 1994). Different spectral parameters (Ni-B, Ni-C, and $g = 2.02$ EPR signals and normalized spectral changes at 410 and 600 nm) were plotted as functions of the number of oxidizing equivalents/mole consumed. The resulting A_{600} titration curves reflected the equivalents/mole of unreacted oxidant, and they allowed the end points of the titrations to be determined. The A_{410} titration curves reflected changes in the redox status of the Fe−S clusters. The Ni-B and Ni-C curves reflected the redox status of the Ni center, and the $g = 2.02$ titration curves reflected the fraction of Fe_3S_4 clusters in the 1+ core oxidation state.

To analyze these titration curves, we have constructed models of the redox reactions occurring in Hase and used them to simulate the curves. We used the results of this analysis to reformulate the proposed catalytic mechanism described earlier, using the concept of redox microstates. In this paper, we describe the analysis, argue that Ni-C is two electrons more reduced than Ni-AB, present a tricyclic mechanism of catalysis, and use that mechanism to suggest that the redox status of one of the $[Fe_4S_4]^{2+/1+}$ clusters controls the reversibility of the catalyzed reaction.

EXPERIMENTAL AND ANALYTICAL PROCEDURES

Midpoint Potential Measurements. Desulfovibrio gigas was grown and Hase was purified and assayed, as described (Barondeau et al., 1994). All procedures involving Hase were performed in an anaerobic glove box (Vacuum/Atmospheres Model HE-453) with an Ar atmosphere and *ca.* 0.5 ppm O_2 (monitored by a Teledyne Model 301 O_2 analyzer).

An electrochemical cell was constructed from an 8 mm o.d. × 6 cm glass tube. The bottom of the tube was sealed and flattened, and a 10/30 outer ground-glass joint was connected to the top. A second tube (0.5 cm o.d. × 2.5 cm) was attached orthogonal to the first, 1.5 cm from the bottom. A shortened EPR tube (0.5 cm o.d. × 4 cm), as described by Shin and Lindahl (1992), was connected to the open end of the orthogonal extension using latex tubing. A third tube (0.5 cm o.d. × 6.5 cm) was attached to the first tube 4 cm from the bottom and pointed upward at a 45° angle. A double-septum seal formed the distal end of the third tube.

An Au working electrode was prepared by inserting Au wire through a capillary tube (1 mm × 12.4 cm), such that the end of the wire extended 3 mm from the end of the capillary. The interface of the tube and the wire was sealed with epoxy. An Ag/AgCl reference electrode was prepared by sealing a piece of "thirsty glass" (Corning) with epoxy into the bottom of a glass tube (0.3 cm o.d. × 12 cm), inserting an Ag wire (whose surface was oxidized at a current density of 0.4 mA/cm^2 for 30 min using 0.1 M HCl and then aged for several days) into the tube, and filling the tube with a saturated KCl/AgCl solution. The reference and working electrodes were sealed with epoxy into a 10/30 inner ground-glass joint. The electrode assembly was attached to the electrochemical cell through the outer ground-glass joint at the top, such that the electrodes extended to within 1 cm of the bottom of the cell. The reference electrode was calibrated from the $E_{1/2}$ obtained from the cyclic voltammogram of methyl viologen (assumed to be −440 mV vs NHE). Potentials were set using a potentiostat (Princeton Applied Research Model 273).

To determine the midpoint potential of Ni-SI/Ni-C, the redox mediators anthroquinone-1,2-disulfonate ($E_m = -184$ mV), neutral red ($E_m = -325$ mV), phenosafranine ($E_m = -252$ mV), benzyl viologen ($E_m = -348$ mV), and methyl viologen ($E_m = -440$ mV) were added to a sample of H_2-free Hase (4.5 mL of 31 μM Hase; specific activity, 610 units/mg; 50 μM concentration of each mediator). The solution was reduced by adding 175 μL of H_2-saturated water. After 0.5 h, 0.44 mL aliquots were transferred to the cell. The potentials of the stirred solution were increased by adding incremental volumes of 2.5 mM thionin by syringe injection through the double-septum seal of the cell. After each addition, the solution was momentarily transferred (by turning the cell 90° and gently tapping the solution) into the EPR tube attached to the side arm of the cell. The solution was transferred back to the bottom of the cell and the potential was remeasured. Samples were rapidly frozen in the EPR tubes 5−10 min after solution potentials drifted less than 1 mV/min.

The same procedure was used to determine the midpoint potential of the Ni-B/Ni-SI couple. The mediators used included thionin ($E_m = +60$ mV), methylene blue ($E_m = +37$ mV), 2,5-dihydroxyl-*p*-benzoquinone ($E_m = -60$ mV), Indigo carmine ($E_m = -125$ mV), and anthroquinone-2,6-disulfonate ($E_m = -184$ mV). The final mediator concentrations were 40 μM each. The final enzyme (specific activity, 1100 units/mg) concentration was *ca.* 30 μM.

Description of the TED Model. The primary model used to simulate the titrations assumes that Ni-C is two electrons more reduced than Ni-AB. The model, called the two-electron-difference model, or TED, is defined by eqs 1−6:

$$2\text{Ni-R} + T_{ox} \rightleftharpoons 2\text{Ni-C} + T_{red} \quad (1)$$

$$2\text{Ni-C} + T_{ox} \rightleftharpoons 2\text{Ni-SI} + T_{red} + 2H^+ \quad (2)$$

$$2\text{Ni-SI} + T_{ox} \rightleftharpoons 2\text{Ni-B} + T_{red} \quad (3)$$

$$2[Fe_{4a}]^{1+} + T_{ox} \rightleftharpoons 2[Fe_{4a}]^{2+} + T_{red} \quad (4)$$

$$2[Fe_{4b}]^{1+} + T_{ox} \rightleftharpoons 2[Fe_{4b}]^{2+} + T_{red} \quad (5)$$

$$2[Fe_3]^{0} + T_{ox} \rightleftharpoons 2[Fe_3]^{1+} + T_{red} \quad (6)$$

TED specifies that Hase contains three $n = 1$ redox species (the Fe−S clusters) and one species that undergoes three sequential $n = 1$ redox reactions (the Ni center). T_{ox} and

T_{red} represent the oxidized and two-electron-reduced forms of the oxidant (thionin), respectively. The reactions are not meant to imply a particular mechanism (we are not proposing that the oxidant reacts directly with all centers in Hase), only that equilibrium conditions between each center and the oxidant can be established.

The three $n = 1$ redox species (the Fe−S clusters) are assumed to absorb at 410 nm in their oxidized (ϵ_{ox}) and reduced (ϵ_{red}) forms. It is also assumed that $\epsilon_{ox} > \epsilon_{red}$ for each cluster and that the molar extinction coefficient differences, $\Delta\epsilon = \epsilon_{ox} - \epsilon_{red}$, are the same for each cluster. A_{410} is presumed to be unaffected by the redox state of the Ni center for reasons mentioned earlier (Barondeau et al., 1994). Fully reduced Hase, obtained in 1 atm of H_2, yielded a minimum A_{410} (A_{min}), while the fully oxidized samples at the end points of the titrations, where the Fe−S clusters are fully oxidized, yielded the maximum A_{410} (A_{max}). The A_{410} titration curve at any point of the titration is defined by $(A_{410} - A_{min})/(A_{max} - A_{min})$. Given the assumptions of the model, this normalized fractional change at 410 nm is related to the concentrations of the three Fe−S clusters according to

$$\frac{(A_{410} - A_{min})}{(A_{max} - A_{min})} = \frac{[Fe_{4a}]^{2+} + [Fe_{4b}]^{2+} + [Fe_3]^{1+}}{[Fe_{4a}]_{tot} + [Fe_{4b}]_{tot} + [Fe_3]_{tot}} \quad (7)$$

TED assumes that the Ni center has four stable states, Ni-AB, Ni-SI, Ni-C, and Ni-R, each separated from adjacent states by one electron:

$$\text{Ni-AB} \underset{-e^-}{\overset{+e^-}{\rightleftharpoons}} \text{Ni-SI} \underset{-e^- - H^+}{\overset{+e^- + H^+}{\rightleftharpoons}} \text{Ni-C} \underset{-e^-}{\overset{+e^-}{\rightleftharpoons}} \text{Ni-R}$$

TED is derived from models (Cammack et al., 1987; Teixeira et al., 1989; Huang et al., 1993) in which Ni-AB was proposed to be Ni^{3+}, Ni-SI was Ni^{2+}, Ni-C was $Ni^{1+}(H^+)$ or Ni^{3+}-H^-, and Ni-R was Ni^{2+}-H^- or $Ni^{2+}(\eta^2$-$H_2)$. However, TED does not imply a particular designation of any Ni state, nor does it imply that redox reactions occur at the Ni ion *per se*. They may, for example, occur at a ligand of the Ni.

The experimental Ni-C, Ni-B, and $g = 2.02$ signals quantified to significantly less than 1 spin/mol (Barondeau et al., 1994). Such low intensities are common for Hase, but the reason for their occurrence, and whether the EPR-silent Ni ions are redox-active, is not known. To account for all possibilities, the low intensities were interpreted in two ways. The *partial* interpretation, called TED_P, assumes that only the EPR-active Ni ions are redox-active and that the remainder are, for some reason, EPR-silent and redox-inactive (probably as Ni^{2+}). The *total* interpretation, called TED_T, assumes that all Ni ions in the enzyme are redox-active, whether or not they exhibit EPR signals. This assumption seems to require that a fraction of Ni^{3+} or Ni^{1+} ions is spin-coupled to an unknown paramagnet, so as to become EPR-silent.

FED and ZED Models. Two other models were used to simulate the experimental oxidative titration curves. The four-electron-difference model (FED) is identical to TED, except that it assumes Ni-C is four electrons more reduced than Ni-B. This model was chosen because the electronic state of Ni-C has been proposed to be Ni^{1+}-H^- and Ni^{1+}-$(\eta^2$-$H_2)$ (Baidya et al., 1992a; van der Zwaan et al., 1987), which are four electrons more reduced than Ni^{3+}. FED assumes two additional hypothetical Ni states, designated Ni-I1 and Ni-I2. Ni-I2 should be an odd-electronic species, most likely EPR-active. FED does not assume specific designations for the Ni states but, for example, Ni-B could correspond to Ni^{3+}, Ni-SI to Ni^{2+}, Ni-I2 to Ni^{1+}, Ni-I1 to Ni^{2+}-H^-, Ni-C to Ni^{1+}-H^-, and Ni-R to Ni^0-H^-. FED is defined by reactions 8−15.

$$2\text{Ni-R} + T_{ox} \rightleftharpoons 2\text{Ni-C} + T_{red} \quad (8)$$

$$2\text{Ni-C} + T_{ox} \rightleftharpoons 2\text{Ni-I1} + T_{red} \quad (9)$$

$$2\text{Ni-I1} + T_{ox} \rightleftharpoons 2\text{Ni-I2} + T_{red} \quad (10)$$

$$2\text{Ni-I2} + T_{ox} \rightleftharpoons 2\text{Ni-SI} + T_{red} + 2H^+ \quad (11)$$

$$2\text{Ni-SI} + T_{ox} \rightleftharpoons 2\text{Ni-B} + T_{red} \quad (12)$$

$$2[Fe_{4a}]^{1+} + T_{ox} \rightleftharpoons 2[Fe_{4a}]^{2+} + T_{red} \quad (13)$$

$$2[Fe_{4b}]^{1+} + T_{ox} \rightleftharpoons 2[Fe_{4b}]^{2+} + T_{red} \quad (14)$$

$$2[Fe_3]^{0} + T_{ox} \rightleftharpoons 2[Fe_3]^{1+} + T_{red} \quad (15)$$

The zero-electron-difference model (ZED) assumes that Ni-B and Ni-C are isoelectronic (Ni^{3+}). To adhere to the known EPR properties of the Ni center in Hase, a rather complicated series of events was presumed to occur that involves magnetic coupling between the Ni and Fe_{4a} and a protein conformational change effected by the redox status of Fe_{4b}. A similar model has been proposed (Teixeira et al., 1985) and subsequently discounted (Teixeira et al., 1989). According to ZED, Ni-B arises in molecules containing $[Fe_{4a}]^{2+}$ and declines as $[Fe_{4a}]^{2+}$ becomes reduced and coupled to Ni^{3+}. Thus, Ni-SI is present in molecules with $[Fe_{4a}]^{1+}$ and $[Fe_{4b}]^{2+}$. Ni-C develops when a conformational change (induced by the reduction of $[Fe_{4b}]^{2+}$) draws Ni^{3+} away from $[Fe_{4a}]^{1+}$ (thereby breaking the coupling). ZED is defined by eqs 16−22:

$$2\text{Ni-R} + T_{ox} \rightleftharpoons 2\text{Ni-C} + T_{red} \quad (16)$$

$$2[Fe_{4b}]^{1+} + T_{ox} \rightleftharpoons 2[Fe_{4b}]^{2+} + T_{red} \quad (17)$$

$$2[Fe_{4a}]^{1+} + T_{ox} \rightleftharpoons 2[Fe_{4a}]^{2+} + T_{red} \quad (18)$$

$$2[Fe_3]^{0} + T_{ox} \rightleftharpoons 2[Fe_3]^{1+} + T_{red} \quad (19)$$

$$\frac{([Fe_{4a}]^{2+})([Fe_{4b}]^{1+})}{([Fe_{4a}]_{tot})([Fe_{4b}]_{tot})} + \frac{([Fe_{4a}]^{2+})([Fe_{4b}]^{2+})}{([Fe_{4a}]_{tot})([Fe_{4b}]_{tot})} = \frac{(\text{Ni-B})}{(Ni_{tot})} \quad (20)$$

$$\frac{([Fe_{4a}]^{1+})([Fe_{4b}]^{2+})}{([Fe_{4a}]_{tot})([Fe_{4b}]_{tot})} = \frac{(\text{Ni-SI})}{(Ni_{tot})} \quad (21)$$

$$\frac{([Fe_{4a}]^{1+})([Fe_{4b}]^{1+})}{([Fe_{4a}]_{tot})([Fe_{4b}]_{tot})} = \frac{(\text{Ni-C} + \text{Ni-R})}{(Ni_{tot})} \quad (22)$$

The three models (ZED, TED, and FED) were used to simulate the experimental titration curves of Barondeau et al. (1994). Details of the simulation procedure are given in the Appendix.

Table 1: Calibrated Best-Fit Parameters According to TED Models[a]

	titration 1		titration 2		titration 3		titration 4		average		
	partial	total	partial	total	partial	total	partial	total	partial	total	reported[g]
$E'_m([Fe_3S_4]^{1+/0})$[e]	−85	−85	−135	−125	−175	−175	−130	−130	−130	−130	−70[b]
$E'_m([Fe_4S_{4a}]^{2+/1+})$[f]	−350	−350	−325	−370	−265	−270	−300	−305	−310	−325	−350[c,d]
$E'_m([Fe_4S_{4b}]^{2+/1+})$[f]	−370	−380	−360	−380	−355	−350	−330	−335	−355	−360	−410[c,d]
E'_m(Ni-B/Ni-SI)[e]	−150	−150	−150	−150	−150	−150	−150	−150	−150	−150	nd
E'_m(Ni-SI/Ni-C)[f]	−330	−330	−330	−330	−330	−330	−330	−330	−330	−330	−310, −390[d]
E'_m(Ni-C/Ni-R)[f]	−350	−350	−380	−385	−365	−365	−375	−370	−370	−370	−450[d]
ΔE_B	40	25	90	95	75	70	70	30	70	55	
ΔE_C	90	95	65	120	45	50	45	65	60	80	
initial equiv/mol oxidized	0.78	0.75	1.08	1.27	1.06	1.01	0.62	0.99	0.86	1.00	
$Q_{best\text{-}fit}/Q_{min}$	1.00	1.04	1.07	1.00	1.09	1.16	1.07	1.00	1.06	1.05	
$[Hase]_{sim}/[Hase]_{exp}$	1.16	0.92	1.17	0.75	1.29	1.03	1.16	0.75	1.18	0.86	

[a] Potentials are given in millivolts vs NHE at pH 8.0. [b] Teixeira et al., 1983. [c] Teixeira et al., 1989. [d] Cammack et al., 1987. [e] Best-fit value equals the value in the table plus ΔE_B. [f] Best-fit value equals the value in the table plus ΔE_C. [g] Literature values have been adjusted to pH 8.0 for comparison.

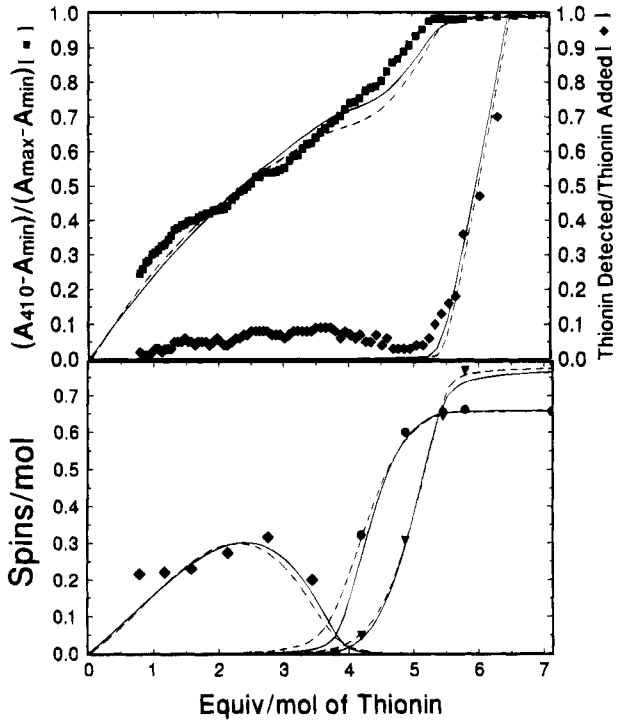

FIGURE 1: Simulation of oxidative titration 1 curves using the TED models. Upper panel: ■, A_{410} titration curve $((A_{410} - A_{min})/(A_{max} - A_{min})$ vs equiv/mol added thionin); ◆, A_{600} titration curve (equiv/mol of detected thionin vs equiv/mol of added thionin). Lower panel: ◆, Ni-C titration curve (spin/mol vs equiv/mol added thionin); ●, Ni-B titration curve; ▼, $g = 2.02$ titration curve. Solid lines in the upper and lower panels are simulations using TED_P; dashed lines are those using TED_T. Fits were obtained using the best-fit midpoint potentials whose calibrated values are given in Table 1. The TED_P and TED_T simulations, respectively, required Hase concentrations 116% and 92% of the experimental value and required that the sample was 0.78 and 0.75 equiv/mol oxidized at the start of the titrations. These adjustments have been made in the simulations shown.

RESULTS AND DISCUSSION

Simulations Using the TED Models. The TED models were evaluated according to their ability to simulate the distinctive shapes of the experimental titration curves. Relative differences between fits were assessed objectively according to the Q_{fit} parameters described in the Appendix. According to the $Q_{best\text{-}fit}/Q_{min}$ ratios, given in Table 1 and as can be seen in Figure 1, both the TED_P and TED_T models afforded excellent simulations of titration 1. The fits to the other three titrations were of comparable quality (available as supplementary material). The TED models were considered acceptable by this criterion.

In fitting the simulations, the Ni redox chemistry was controlled by the shapes of the Ni-B and Ni-C titration curves, while that of the Fe_3S_4 cluster was controlled by the $g = 2.02$ titration curve. The only flexible aspects of the simulations (not specified by EPR signals) were those that affected the two $[Fe_4S_4]^{2+/1+}$ clusters and the Ni-C/Ni-R transition. Thus, the midpoint potentials of the Fe_4S_4 clusters were adjusted solely to fit the A_{410} titration curve. E_m' for the Ni-C/Ni-R couple was the least certain of all, because it was controlled only by the shape and intensity of the first part of the Ni-C titration curve. The best-fit simulations were a compromise between all of these factors. The most noticeable difference between the simulated vs experimental curves was the shape of the A_{410} titration curve; the experimental curve was devoid of a noticeable plateau region, while the simulated ones exhibited slight plateaus 1−2 equiv/mol before the end point. Since the models assume that only redox changes in the Fe−S clusters contribute to changes in A_{410}, plateaus arise in the simulations when the Ni center undergoes redox chemistry and the Fe−S clusters do not.

The second criterion used to evaluate the simulations was how similar the best-fit enzyme concentrations were to the experimentally determined values. This can be assessed from the $[Hase]_{sim}/[Hase]_{exp}$ ratios in Table 1. The best-fit TED_P simulation of titration 1 required an enzyme concentration 16% greater than the experimental concentration, while that for TED_T required an enzyme concentration 8% lower than the experimental value. Enzyme concentrations are very difficult to determine with high precision, and those for the titrations were estimated to have uncertainties of ±20% (Barondeau et al., 1994). Because the best-fit $[Hase]_{sim}$ values of TED_P and TED_T were within these limits, whether EPR-silent Ni ions are redox-active could not be determined. We favor the partial assumption because it appears to be simpler than the total assumption.

Calibration of Best-Fit Midpoint Potentials. Stoichiometric oxidative titrations cannot directly yield accurate midpoint potentials; they yield only midpoint potential differences between sites having midpoint potentials within *ca.* 0.1 V of each other.[2] To calibrate the potentials obtained from the simulations, we potentiometrically titrated Ni-C to Ni-SI and Ni-SI to Ni-B, using the same conditions that were

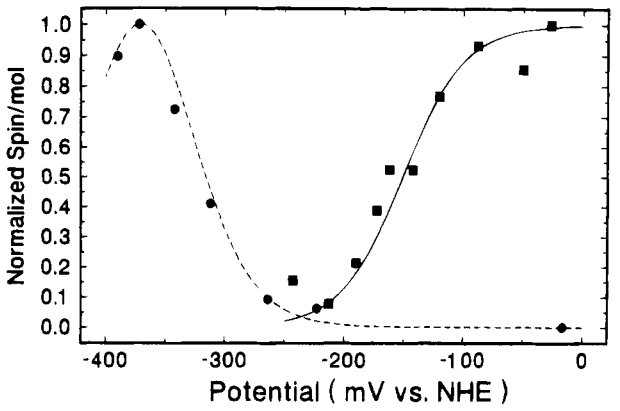

FIGURE 2: Midpoint potentials of the Ni-B/Ni-SI and Ni-SI/Ni-C couples: ●, Ni-C EPR signal intensity; ■, Ni-B EPR signal intensity. The titrations were performed as described in Experimental and Analytical Procedures. The dashed line near the circles is the best fit to [Ni-C]/{[Ni-SI] + [Ni-C] + [Ni-R]} = 1/{exp[(E − E_{m1})nF/RT] + exp[(E_{m2} − E)nF/RT + 1}, where E_{m1} is the best-fit midpoint potential (−330 mV) for the Ni-SI/Ni-C couple, E_{m2} is that for the Ni-C/Ni-R couple (−410 mV), and E is the measured potential. The solid line near the squares is the best fit to [Ni-B]/{[Ni-B] + [Ni-SI]} = exp[(E_{m3} − E)nF/RT, where E_{m3} is the best-fit midpoint potential for the Ni-B/Ni-SI couple (−150 mV).

used in the oxidative titrations (except that mediators were present). The results, shown in Figure 2, indicate midpoint potentials (obtained in the oxidative direction) of −330 ± 25 and −150 ± 25 mV vs NHE at pH 8.0 for the Ni-SI/Ni-C and Ni-B/Ni-SI couples, respectively. The E_m' for the Ni-SI/Ni-C couple is similar to that measured by Teixeira et al. (1989), while that for the Ni-B/Ni-SI couple has not been reported. We set the best-fit midpoint potentials of the Ni-SI/Ni-C couples in each simulation to −330 mV and adjusted the potentials of the three other couples that were within 0.1 V of this value (Ni-C/Ni-R, $[Fe_{4a}]^{2+/1+}$, and $[Fe_{4b}]^{2+/1+}$) accordingly. We also set the best-fit E_m' of the Ni-B/Ni-SI couples to −150 mV and adjusted the potentials of the $[Fe_3S_4]^{1+/0}$ cluster accordingly. The best-fit calibrated E_m' values obtained in this manner are listed in Table 1. Their deviation from reported experimental values represents a third criterion used to evaluate the TED models. Since the calculated and experimental values are adequately similar, the TED models are acceptable according to this criterion.

Simulations Using the ZED and FED Models. We attempted to simulate the data using the ZED and FED models (see Experimental and Analytical Procedures). The best-fit simulations of titration 1 using ZED are shown in Figure 3. ZED is excluded by the three criteria mentioned earlier, since the shapes of the simulations did not fit the experimental curves, the enzyme concentrations required by the simulations were not within 20% of the experimental

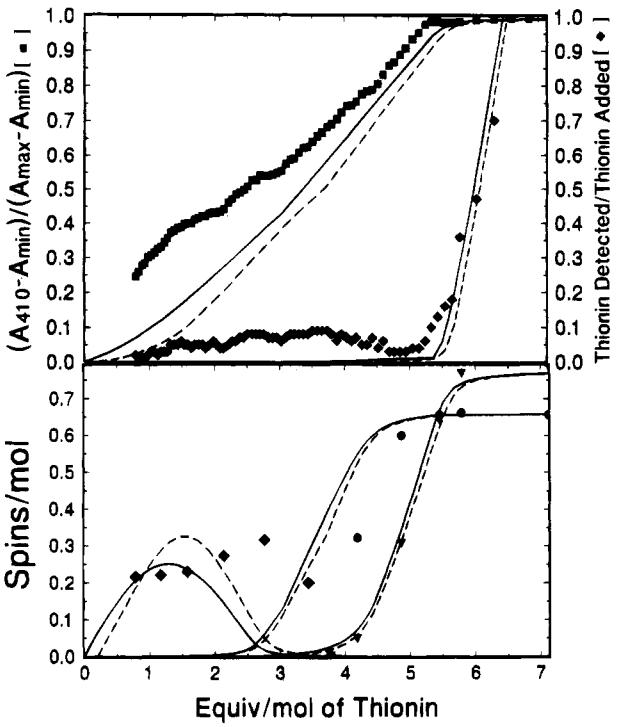

FIGURE 3: Simulation of oxidative titration 1 curves using the ZED models. Plots are similar to those of Figure 1. The calibrated best-fit midpoint potentials were $E_m'([Fe_3S_4]^{1+/0})$ = −0.05 V; E_m'-($[Fe_{4a}]^{2+/1+}$ same as Ni-B/Ni-SI) = −0.15 V; $E_m'([Fe_{4b}]^{2+/1+}$ same as Ni-SI/Ni-C) = −0.30 V (ZED_P) and −0.28 V (ZED_T); E_m' (Ni-C/Ni-R) = −0.325 V (ZED_P) and −0.315 V (ZED_T). The ZED_P and ZED_T simulations, respectively, required Hase concentrations 192% and 175% of the experimental value and required that the sample titrated was 0.78 and 0.58 equiv/mol oxidized at the start of the titrations. These adjustments have been made in the simulations shown. The Q_{fit}/Q_{min} ratios were 2.4 for both ZED_P and ZED_T.

values, and the calibrated best-fit midpoint potentials significantly deviated from published values.

The best-fit simulations using FED are shown in Figure 4. FED_T can be excluded because the enzyme concentrations required by the simulations differed from the experimental values by more than 20%. The required best-fit enzyme concentration for FED_P was near the experimental value, essentially because the additional oxidizing equivalents assumed to be associated with the Ni by the FED model are offset by the assumption that only EPR-active Ni species are redox-active. The shapes of the simulated curves obtained using the FED models fit the experimental curves adequately, although not as well as those obtained using the TED models; $Q_{best\text{-}fit}$ values for the FED simulations of titration 1 were *ca.* 140% of Q_{min}. FED simulations tended to exhibit a more significant plateau region in the A_{410} curve and a Ni-C curve that was shifted relative to the data. Both patterns arise because of the assumption by FED that the Ni center undergoes two additional n = 1 redox reactions relative to what is assumed by TED.

Basically, due to the uncertainties in the titration data itself (20% uncertainty in the concentrations of the samples, uncertainty as to whether EPR-silent Ni ions are redox-active, and uncertainty in knowing the exact redox status of the samples at the beginning of the titrations), models similar to TED but with an additional n = 1 redox site probably *could not* be excluded according to our criteria. Models similar to TED but with two additional n = 1 redox sites

[2] Let E_{mA} and E_{mOx} be the respective midpoint potentials of a site A and the oxidant Ox used to titrate A. If E_{mA} is more than *ca.* 0.1 V more negative than E_{mOx}, A will react stoichiometrically with Ox, yielding a linear titration curve with a sharp end point. E_{mA} cannot be determined accurately from such a curve. If E_{mA} is within *ca.* 0.1 V of E_{mOx}, A will react nonstoichiometrically (it will exist in equilibrium with Ox), yielding a nonlinear titration curve that can be fit to yield E_{mA}. If two stoichiometrically oxidizable sites (A and B) are titrated and $|E_{mA} - E_{mB}| = \Delta E_m >$ *ca.* 0.1 V, the site with the more negative E_m will oxidize first. But if $\Delta E_m <$ *ca.* 0.1 V, they will titrate in a manner that is sensitive to ΔE_m (but not to E_{mA} or E_{mB}). In Hase, the Ni-B/Ni-SI and $[Fe_3S_4]^{1+/0}$ couples are related in this manner, as are the Ni-SI/Ni-C, Ni-C/Ni-R, $[Fe_{4a}]^{2+/1+}$, and $[Fe_{4b}]^{2+/1+}$ couples.

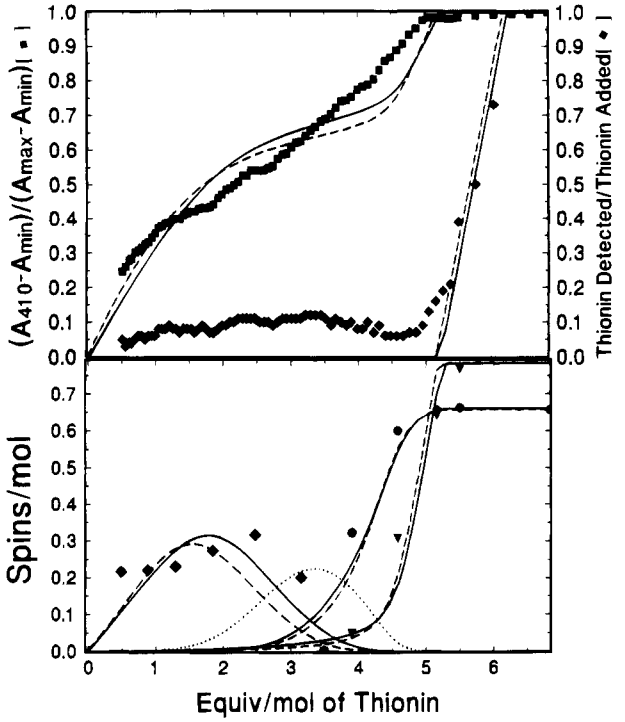

FIGURE 4: Simulation of oxidative titration 1 curves using FED models. Plots are similar to those of Figure 1. The dotted line is a simulation of the titration curve of the unobserved species Ni-I2. The calibrated best-fit midpoint potentials were $E_m'([Fe_3S_4]^{1+/0}) = -0.075$ V (FED_P and FED_T); $E_m'([Fe_{4a}]^{2+/1+}) = -0.380$ V (FED_P) and -0.375 V (FED_T); $E_m'([Fe_{4b}]^{2+/1+}) = -0.380$ V (FED_P) and -0.390 (FED_T); E_m'(Ni-B/Ni-SI) $= -0.150$ V (FED_P and FED_T); E_m'(Ni-SI/Ni-I2) $= -0.220$ V (FED_P) and -0.330 V (FED_T); E_m'(Ni-I2/Ni-I1) $= -0.230$ V (FED_P) and -0.330 V (FED_T); E_m'(Ni-I1/Ni-C) $= -0.330$ V (FED_P and FED_T); E_m'(Ni-C/Ni-R) $= -0.370$ V (FED_P) and -0.365 V (FED_T). The FED_P and FED_T simulations, respectively, required Hase concentrations 86% and 65% of the experimental value and required that the sample titrated was 0.49 equiv/mol oxidized at the start of the titration. These adjustments have been made in the simulations shown. The $Q_{best\text{-}fit}/Q_{min}$ ratios for FED_P and FED_T were 1.33 and 1.44, respectively.

(or with one $n = 2$ site) probably *could* be excluded. This delimits the total number of possible redox reactions (including those that do not exhibit a measurable spectroscopic property) occurring in the enzyme between *ca.* -350 and $+100$ mV, the potentials accessed during the titrations.

Improbability of FED Models. FED models can be further discounted because the number of Ni electronic states assumed by FED is chemically unreasonable and the differences between the best-fit calibrated E_m' values for adjacent Ni couples are unrealistically small (see Figure 4 legend). The Ni center in Hase is unprecedented in its ability to undergo a large number of magnetic transitions (Ni-R → Ni-C → Ni-SI → Ni-AB) within a small potential range (*ca.* 300 mV). According to TED, these transitions correspond to three redox steps, such as Ni^{2+}-H^- → $Ni^{1+}(H^+)$ → Ni^{2+} → Ni^{3+}. According to FED, they correspond to five steps, such as Ni^0-H^- → Ni^{1+}-H^- → Ni^{2+}-H^- → Ni^{1+} → Ni^{2+} → Ni^{3+}. The redox potentials for well-characterized $Ni^{2+/1+}$ complexes are *ca.* 2 V below those for the corresponding $Ni^{3+/2+}$ couples (Gore & Busch, 1973; Lovecchio et al., 1974). How could the Ni center in the enzyme span so many states (four for TED and six for FED) within such a small potential range, using biological ligands, while well-characterized Ni complexes span fewer states over a much greater range? This highly improbable requirement provides a strong argument against the FED models.

A second basis for excluding FED models is that they predict a species that is expected to be EPR-active but has not been observed. A signal, from a state designated Ni-I2 in the FED model (one designation for which would be Ni^{1+}), should have developed as Ni-SI (Ni^{2+}) is reduced and before Ni-C (Ni^{1+}-H^-) develops. The best-fit FED_P simulation of titration 1 indicates that this species would be present in detectable amounts if it existed (Figure 4, lower panel, dotted line). However, no EPR signal arising from such a species has been observed [Figure 4 of Barondeau et al. (1994)].

FED-based models appear to have been proposed to explain the CO-binding, EPR, photochemical, and proton hyperfine coupling properties of Ni-C. CO binds to the Ni-C state (to the Ni directly) but not to Ni-AB (DerVartanian et al., 1985; van der Zwaan et al., 1986, 1990). In related model compounds, CO binds to Ni^{1+}, but not to Ni^{2+} or Ni^{3+} (Baidya et al., 1992a,b). This would appear to indicate a Ni^{1+} designation for Ni-C. Van der Zwaan et al. (1986) found that the CO-bound form of hydrogenase is photosensitive and that the EPR signal produced by photolyzing it is *virtually the same* as that produced by photolyzing Ni-C. The photodissociation of carbonyls from metal complexes is well-known (Geoffroy & Wrighton, 1979), and that occurring in Hase probably yields Ni^{1+} and free CO. Thus, the photolysis product of Ni-C is probably Ni^{1+} as well. Recently, using ENDOR spectroscopy, Whitehead et al. (1993) found that a hydrogenic species (H^+, H^-, or H_2) was cleaved during the photolysis of Ni-C. Taken in conjunction with the CO-binding studies, Ni-C would appear to be either $Ni^{1+}(H^+)$, Ni^{1+}-H^-, or $Ni^{1+}(\eta^2\text{-}H_2)$.

Van der Zwaan et al. (1987) suggested a $Ni^{1+}(\eta^2\text{-}H_2)$ designation for Ni-C because, in contrast to other hydrides, the photolytic hydrogenic species associated with Ni-C is not coupled strongly to the electronic spin. They expected a molecular hydrogen species to exhibit weaker coupling than a hydride.

Baidya et al. (1992a) proposed a Ni^{1+}-H^- designation of Ni-C on the basis of the properties of [Ni(2,6′:2′,6″-terpyridine)(2,6-$(Me)_2C_6H_3S)_2$]^0, a model complex of the Ni site in Hase. The complex contains Ni^{2+} in a five-coordinate N_3S_2 trigonal pyramidal geometry and would appear to correspond to the Ni-SI state. The complex can be reduced by one electron to yield a Ni^{1+} species with an EPR signal ($g_{\|} = 2.249$ and $g_{\perp} = 2.126$). (According to the FED interpretation, this state would correspond to Ni-I2, the state that has not been observed in enzyme titrations.) The Ni^{1+} complex can bind hydride to yield a Ni^{1+}-H^- species that exhibits an EPR signal ($g_1 = 2.236$, $g_2 = 2.192$, $g_3 = 2.045$) similar to that of Ni-C ($g_1 = 2.19$, $g_2 = 2.16$, $g_3 = 2.02$). This similarity was used as evidence to assign Ni^{1+}-H^- to Ni-C, but such evidence is tenuous.[3] The Ni^{1+} complex also reacts with CO to yield an EPR-active Ni^{1+}-CO state, which is thought to be equivalent to Ni-C after exposure to CO.

In summary, FED-based models (i) yield simulations with shapes that fit the data more poorly than those obtained

[3] Both Ni^{1+} and Ni^{3+} complexes can yield Ni-C-like signals (Teixeira et al., 1985, 1989; Salerno, 1988). For example, the EPR signal from a $Ni^{3+}(N_2S_2)$ complex ($g_1 = 2.29$, $g_2 = 2.11$, $g_3 = 2.04$) of Krüger and Holm (1987) and a $Ni^{1+}(S_4)$ complex ($g_1 = 2.260$, $g_2 = 2.207$, $g_3 = 2.035$) of Bowmaker et al. (1982) are both similar to Ni-C.

assuming TED; (ii) require that an unrealistically large number of Ni redox states be stable within an unrealistically small potential range; and (iii) predict a species that has not (but should have) been observed spectroscopically. Thus, although FED-based designations of Ni-C, such as Ni^{1+}-H^- and $Ni^{1+}(\eta^2$-$H_2)$, readily explain the CO-binding properties of the Ni center and are compatible with evidence that Ni-C contains a photolabile hydrogenic species, they are probably incorrect. Designations of the Ni center in Hase should be restricted to those that are TED-based.

Compatibility of a TED-Based Model with Reported Properties of the Enzyme. Within the TED framework, the protonated Ni^{1+} designation of Ni-C (Cammack et al., 1987) appears to be most compatible[4] with the established[5] relevant properties of the Ni center. Cammack et al. (1987) reported that E_m' for the Ni-SI/Ni-C couple declined by 120 mV/pH unit, suggesting that Ni-SI binds two protons as it is reduced. The Ni in Hase is almost certainly coordinated by at least two cysteine thiolates (Voordouw, 1992). The unusually mild E_m' for the Ni-SI/Ni-C couple (nominally $Ni^{2+/1+}$) and the small difference in E_m' values between that couple and the Ni-AB/Ni-SI ($Ni^{3+/2+}$) couple might arise because the two protons associated with the reduction of Ni^{2+} to Ni^{1+} bind two cysteine thiolates to form thiols (Shoner et al., 1994), which would stabilize Ni^{1+} (Farmer et al., 1993).

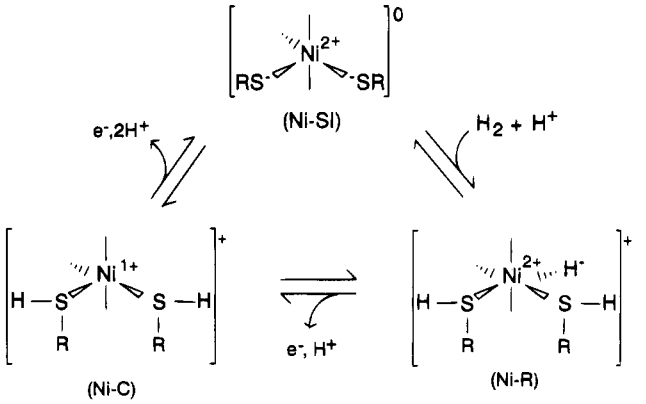

FIGURE 5: Proposed states of the Ni center in Hase during a catalytic cycle. See text for details.

Cammack et al. (1987) found that E_m' for the reduction of Ni-C to Ni-R declined by 60 mV/pH unit, indicating that a third proton associates with the Ni center during this reduction. This proton might bind Ni^{1+} to afford Ni^{2+}-H^- after the one-electron reduction. In this case, E_m' for the Ni-C/Ni-R couple might be unusually mild because the unfavorable reduction of Ni^{1+} couples to a favorable protonation step. Ni-R and Ni-SI are thought to be in redox equilibrium with H_2, but to return to the Ni-SI state, this equilibrium would need to occur with the loss of a proton. These reactions, indicated graphically in Figure 5, constitute a reformulation of the catalytic mechanisms of Cammack et al. (1987), Teixeira et al. (1989), Huang et al. (1993), and Kovacs (1994). Our reformulation assumes that the only Ni state capable of spontaneously oxidizing H_2 to protons is Ni-SI (Fernandez et al., 1986) and that the only Ni state capable of spontaneously reducing protons to H_2 is Ni-R (Barondeau et al., 1994).

Using this same designation of Ni states, the photolytic reaction of Ni-C might correspond to the deprotonation of one or both thiols. The indirect association of the photolabile hydrogenic species with the Ni ion rationalizes the relatively weak proton hyperfine coupling associated with the electronic spin (Fan et al., 1991; Whitehead et al., 1993). To make the photolytic product of Ni-C and the CO-bound form of Ni-C equivalent, photolysis of the CO-bound form might involve both the loss of protons as well as CO.

Redox Microstates of Hase. The best-fit TED_P simulation of titration 1 can be decomposed into the redox states of every species present in Hase (Figure 6). These species can also be described with the concept of redox microstates (Palmer & Olson, 1980), which are sets of specific redox states of the four redox centers in the enzyme. With one redox center that has four states and three redox centers with two states, Hase has a total of 32 ($4 \times 2 \times 2 \times 2$) redox microstates. We will consider only those that may be part of the catalytic mechanism of the enzyme. At pH 8, E_m' for the H_2/H^+ couple is -480 mV, while E_m' for the external electron acceptor used for assays, benzyl viologen, is -348 mV. Thus, the centers used in a redox capacity during catalysis will most likely have midpoint potentials near these limits. Because the midpoint potentials of the $[Fe_3S_4]^{1+/0}$ and Ni-B/Ni-SI couples are significantly outside this range, the Fe_3S_4 cluster and the Ni-B state probably do not undergo redox during catalysis. Moreover, Ni-B does not appear to be capable of binding H_2 (Cammack et al., 1987; Fernandez et al., 1985; Hallahan et al., 1986). Consequently, we will

[4] The CO-binding properties are more difficult to explain if the Ni^{3+} hydride designation of Ni-C is assumed, for why would CO bind Ni-C but not bind well-characterized Ni^{3+} model complexes? We considered that CO binding induces an internal electron-pair transfer from the hydride to Ni^{3+}, yielding Ni^{1+}-CO and H^+. CO binding is known to increase the acidity of metal hydrides (Kristjansdottir & Norton, 1992). Moreover, the Ni^{2+} Schiff base macrocycle formed by the template condensation of 2,6-diacetylpyridine with 3,3′-iminobis(propylamine) in $NiCl_2$ can be reduced by one electron to afford a ligand-based radical species $Ni^{2+}(L^{\bullet})$ with a single isotropic EPR signal at $g = 2.002$ (Lewis & Schröder, 1982). When CO binds to this complex, the EPR signal changes to $g_{\|} = 2.211$ and $g_{\perp} = 2.050$, suggesting a $Ni^{1+}CO(L^+)$ designation. However, if this chemistry occurred in Hase, CO and H^- would need to bind Ni simultaneously. This would suggest either a four-coordinate Ni-SI state (rather than the more likely five-coordinate complex) or that one of the proteinaceous ligands dissociates so that CO can bind. Another complication with the Ni^{3+}-H^- designation of Ni-C is that the observed hyperfine coupling of the photolabile hydrogenic species is not nearly as strong as that expected for a hydride. To explain this, the hydride would have to be coordinated at an equatorial, not axial, position (Fan et al., 1991; Huang et al., 1993). The CO-binding properties of the enzyme are even more difficult to reconcile with the $Ni^{3+}(\eta^2$-$H_2)$ designation of Ni-C, because it seems less likely that CO binding would induce an electron-pair transfer from H_2 to Ni^{3+} and more likely that H_2 would be displaced (leaving Ni^{3+} to bind CO).

[5] Bagyinka et al. (1993) and Whitehead et al. (1993) recently reported that the Ni X-ray absorption edge for all of the Ni states (Ni-A, Ni-B, Ni-SI, Ni-C, Ni-R, and the photolyzed product of Ni-C) were very similar, and they concluded that the Ni ion is in the same oxidation level in every state and that different redox forms of an unspecified ligand to the Ni are responsible for the different Ni states. This conclusion is quite controversial and requires further experimental support before it can be considered established. At issue is whether well-characterized Ni^{1+}, Ni^{2+}, and Ni^{3+} model compounds actually exhibit the shift in edge energy anticipated by these conclusions. These conclusions also render the other known properties of the Ni center difficult to explain. For example, if Ni-AB and Ni-C were both Ni^{3+}, CO should not bind to either state; if they were both Ni^{1+}, CO should bind to both. Since some Ni^{2+} organometallic compounds bind CO (Saint-Joly et al., 1980), Whitehead et al. (1993) suggested Ni^{2+} for all states. But a redox-inactive Ni^{2+} state does not appear to be compatible with the metal-based character of Ni-A, Ni-B, and Ni-C EPR signals (Teixeira et al., 1989; Salerno, 1988).

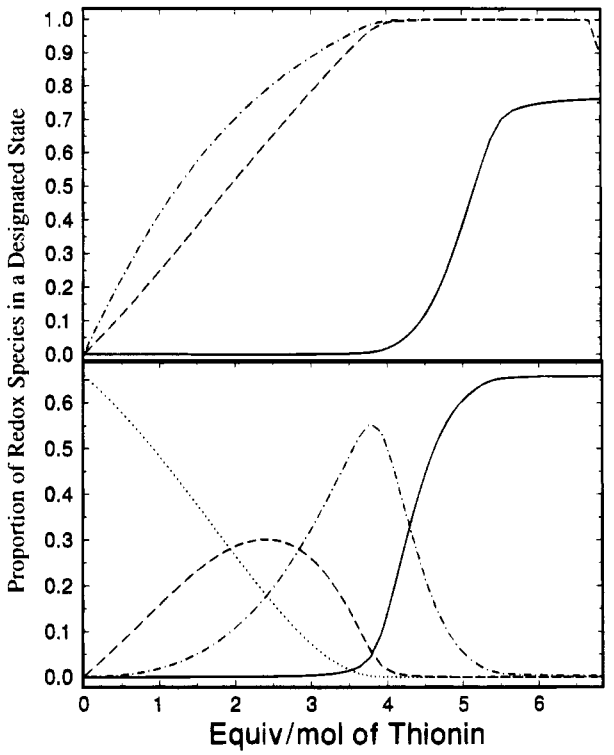

FIGURE 6: Decomposition of the best-fit TED_P simulation of titration 1. Lines indicate the proportion of Hase in a given species during titration 1. Upper panel: dashed-dotted-dashed line, $[Fe_{4b}]^{2+}$; dashed line, $[Fe_{4a}]^{2+}$; solid line, $[Fe_3]^{1+}$. Lower panel: dotted line, [Ni-R]; dashed line, [Ni-C]; dashed-dotted-dashed line, [Ni-SI]; solid line, [Ni-B].

consider only those microstates involving reduced $[Fe_3S_4]^0$ clusters and Ni in the Ni-SI, Ni-C, or Ni-R states.

The remaining 12 catalytically relevant redox microstates will be designated by alphanumeric symbols of the form N*ba*, where N designates the state of the Ni center (N = R, C, or S according to whether it is in the Ni-R, Ni-C, or Ni-SI state, respectively), *b* designates the core oxidation state of Fe_{4b} (b = 2 for $[Fe_{4b}]^{2+}$ and 1 for $[Fe_{4b}]^{1+}$), and *a* designates the core oxidation state of Fe_{4a} (a = 2 for $[Fe_{4a}]^{2+}$ and 1 for $[Fe_{4a}]^{1+}$). For example, what we previously called fully reduced enzyme (Barondeau et al., 1994) corresponds to the microstate R11 (Ni-R, $[Fe_{4b}]^{1+}$, and $[Fe_{4a}]^{1+}$). The state we called the start point of the oxidative titrations, obtained by removing H_2 from R11, corresponds to a mixture of microstates C12 and C21, since it exhibited the Ni-C EPR signal and had partially oxidized (16−38%) Fe−S clusters. Finally, the state we called the null point corresponds to the microstate S22, since the Ni center was in the Ni-SI state and Fe_{4b} and Fe_{4a} were both oxidized (the Fe_3S_4 cluster was reduced).[6]

The relative population of a microstate at a given potential (or point in the oxidative titrations) is determined by the set of midpoint potentials for the redox couples. The relative population of C12 at a given potential, for example, would be the normalized product [Ni-C] × $[Fe_{4b}]^{1+}$ × $[Fe_{4a}]^{2+}$ (Prince & Adams, 1987), where [Ni-C], $[Fe_{4b}]^{1+}$, and $[Fe_{4a}]^{2+}$

[6] This nomenclature is easily expanded to include the redox status of the Fe_3 cluster and the Ni-B state of the Ni center. For example, B221 (fully oxidized enzyme) would indicate Ni-B, $[Fe_{4b}]^{2+}$, $[Fe_{4a}]^{2+}$, and $[Fe_3]^{1+}$. B220 would indicate the same states, except $[Fe_3]^0$.

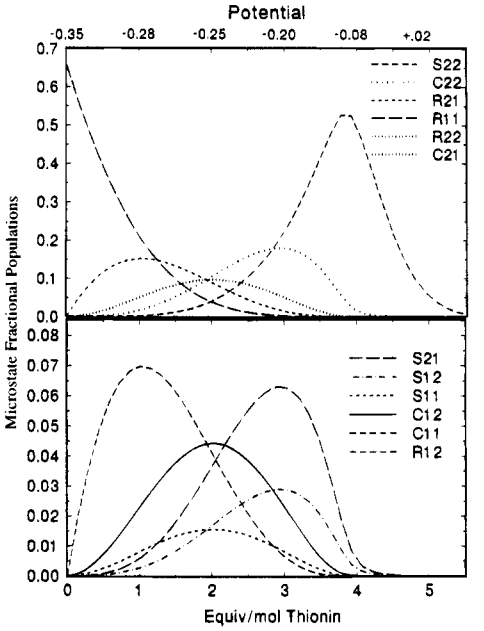

FIGURE 7: Redox microstates according to the best-fit TED_P simulation of titration 1. Lines indicate the proportion of Hase in a given microstate during titration 1. Potentials were calculated as described in the Appendix.

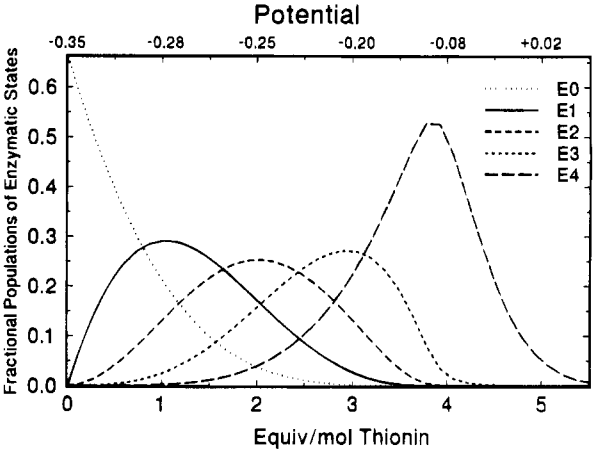

FIGURE 8: Electronic states of Hase according to the best-fit TED_P simulation of titration 1. Lines indicate the proportion of Hase in a given electronic state during titration 1.

are the best-fit concentrations, according to TED_P, at that potential. The relative populations of the 12 catalytically relevant microstates at different points of the titrations and at different calculated potentials are given in Figure 7.

Microstate Description of the Catalytic Mechanism. We can reformulate the catalytic mechanism further using the microstate concept. Besides assuming that only Ni-SI can bind and oxidize H_2, we will assume that Fe_{4b} transfers electrons between the Ni center and Fe_{4a} and that Fe_{4a} transfers them between Fe_{4b} and external redox agents. The catalytically relevant microstates can be organized into five isoelectronic groups called electronic states, designated E_0−E_4 in eqs 23−27, and displayed in Figure 8.

$$E_4 = \{S22\} \quad (23)$$

$$E_3 = \{S21, S12, C22\} \quad (24)$$

$$E_2 = \{S11, C21, C12, R22\} \quad (25)$$

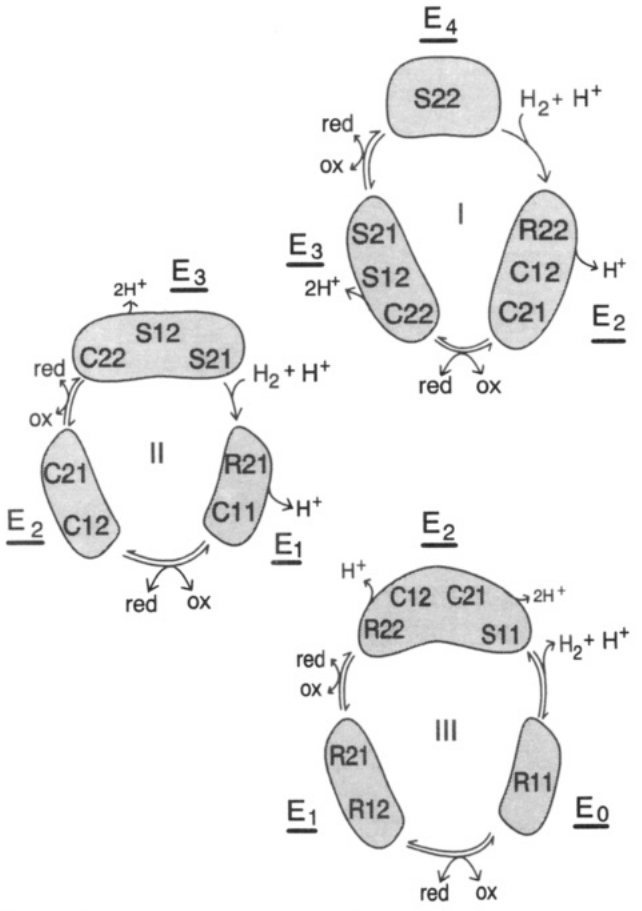

FIGURE 9: Microstate description of the tricyclic mechanism of Hase. Cycle I: S22 reacts with H_2, forming R22. An electron from Ni-R is transferred first to $[Fe_{4b}]^{2+}$ (forming C12), then to $[Fe_{4a}]^{2+}$ (forming C21), and then to Ox (forming C22). A second electron from Ni-C is delivered along the same pathway, forming S12, then S21, and finally the initial microstate S22. Cycle II: S21 reacts with H_2 to form R21. An electron from Ni-R is transferred to $[Fe_{4b}]^{2+}$ (forming C11), and an electron from $[Fe_{4a}]^{1+}$ is transferred to Ox, forming C12. A second electron is transferred from $[Fe_{4b}]^{1+}$ to $[Fe_{4a}]^{2+}$ and then to another Ox, forming C22. Finally, an electron transfers from Ni-C to $[Fe_{4b}]^{2+}$ and then to $[Fe_{4a}]^{2+}$, regenerating the original Ni-SI microstate (S21). Cycle III: S11 reacts with H_2 to form R11. An electron transfers from $[Fe_{4a}]^{1+}$ to Ox (forming R12), an electron from $[Fe_{4b}]^{1+}$ transfers to $[Fe_{4a}]^{2+}$ (forming R21), an electron transfers from $[Fe_{4a}]^{1+}$ to Ox (forming R22), an electron from Ni-R transfers to $[Fe_{4b}]^{2+}$ (forming C12), an electron transfers from $[Fe_{4b}]^{1+}$ to $[Fe_{4a}]^{2+}$ (forming C21), and finally an electron transfers from Ni-C to $[Fe_{4b}]^{2+}$ (forming the initial microstate S11).

$$E_1 = \{C11, R21, R12\} \quad (26)$$

$$E_0 = \{R11\} \quad (27)$$

The microstates composing an electronic state can be interconverted by internal electron transfers and can be viewed as resonance structures with stabilities proportional to their relative populations. According to the assumptions made, three electronic states (E_2, E_3, and E_4) can bind H_2, while two (E_0 and E_1) cannot.[7] The states that bind H_2 are active oxidants of three independent (although interrelated) catalytic cycles designated I, II, and III and shown in Figure 9. Each cycle involves three electronic states. The generic state E_n reacts with H_2, affording E_{n-2}. E_{n-2} reduces an external electron acceptor (Ox), forming E_{n-1}. E_{n-1} reduces a second Ox, regenerating E_n. These three catalytic cycles are interrelated, as shown in Figure 10. The cycle or cycles that operate during catalysis will be determined by the solution potential. Cycle III involves the most reduced microstates and would operate only at relatively negative potentials. Cycle II would operate under intermediate solution potentials, while cycle I involves more oxidized microstates and would operate only at relatively positive potentials.

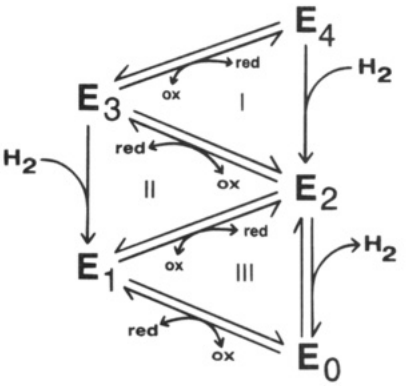

FIGURE 10: Electronic state description of the tricyclic mechanism of Hase. See text for details. For simplicity, the proton balance is not shown.

Only Cycle III Operates Reversibly. Removal of H_2 from fully reduced enzyme (with the Ni in the Ni-R form and the Fe−S clusters reduced) afforded a nearly fully developed Ni-C signal, with Fe−S clusters oxidized by 16−38% at 410 nm (Barondeau et al., 1994). On this basis, we considered Ni-R to be the active reductant of the enzyme (capable of spontaneously reducing protons to H_2). In terms of electronic states, removal of H_2 from E_0 affords E_2, and E_0 is the active reductant. Moreover, E_0 appears to be the *only* active reductant electronic state. If other states were active reductants, the removal of H_2 from E_0 would have afforded electronic states more oxidized than E_2. For example, if E_1 were an active reductant, it would have reacted with H^+ (in the absence of H_2) to yield E_3. If the H_2-free samples had been in the E_3 state, their Fe−S clusters would have been *ca.* 60% oxidized (because E_3 maximizes at 3 equiv/mol thionin, as shown in Figure 8, and at this point, the Fe−S clusters are *ca.* 60% oxidized, as shown in Figure 1). Since the Fe−S clusters were only 16−38% oxidized, and the samples exhibited a strong Ni-C signal, H_2-free samples were most probably in the E_2 state. As a consequence, cycle III appears to operate reversibly (reducing $2H^+$ to H_2 as well as oxidizing H_2 to $2H^+$) because it contains both active reductant (E_0) and active oxidant (E_2) states. Cycles I and

[7] Exposure of oxidized samples to H_2 yields fully reduced Hase in the E_0 state (EPR-silent). According to our proposal, molecules in the E_1 state presumably cannot react with H_2, so that this procedure should have yielded a mixture of E_0 and E_1 (exhibiting Ni-C and partially oxidized Fe_4S_4 clusters). How can this result be explained? One possibility is that the $[Fe_{4a}]^{1+}$ of one molecule can reduce the $[Fe_{4a}]^{2+}$ of another. In that case, two molecules in different microstates of E_1 could disproportionate, and the more oxidized product could react with another H_2:

$$R21 + R12 \rightleftharpoons R22 + R11$$

$$R22 \rightleftharpoons S11 + 3H^+$$

$$S11 + H_2 + H^+ \rightleftharpoons R11$$

$$\text{net: } R21 + R12 + H_2 \rightleftharpoons 2R11 + 2H^+$$

II appear to be capable of oxidizing only H_2 since they contain active oxidant but not active reductant states.

Role of the Fe_4S_4 Clusters in Establishing Reversibility. Viewed from the perspective of the Ni, the three catalytic cycles are essentially identical: Ni-SI reacts with H_2 to yield Ni-R, Ni-R oxidizes by one electron to form Ni-C, and Ni-C oxidizes back to Ni-SI. The cycles differ significantly only in the average redox status of the two Fe_4S_4 clusters. The clusters are more reduced, on average, in cycle III than in cycle II or I.

We propose that the ability of a cycle to operate reversibly requires that the Fe_4S_4 cluster that directly undergoes redox with the Ni, presumed here to be Fe_{4b}, be reduced in the microstate obtained immediately after H_2 reacts (corresponding to R22, R21, and R11 for cycles I, II, and III, respectively). Because Fe_{4b} is reduced in R11 but oxidized in R22 and R21, cycle III may be reversible while cycles I and II may operate only to oxidize H_2.

Viewed mechanistically, Ni-R can reduce either H^+ or $[Fe_{4b}]^{2+}$. When Fe_{4b} is oxidized, Ni-R reduces it and H_2 oxidation ensues. If we assume the designations shown in Figure 5, an electron transfers from Ni^{2+}-H^- to $[Fe_{4b}]^{2+}$, resulting in an acidic Ni^{3+}-H^- transient state that deprotonates to afford Ni-C. On the other hand, when Fe_{4b} is reduced, the hydride of Ni-R attacks the proton on one of the thiols, forming Ni^{2+} (Ni-SI) and H_2.

Conclusion. The oxidative titrations of Barondeau et al. (1994) were simulated using models that assume that Hase contains two $[Fe_4S_4]^{2+/1+}$ clusters, one $[Fe_3S_4]^{1+/0}$ cluster, and one Ni complex stable in four magnetic states (Ni-AB, Ni-SI, Ni-C, and Ni-R). At issue was whether Ni-C was zero, two, or four electrons more reduced than Ni-AB, a state known to arise from a Ni^{3+} species. Models assuming that it was two electrons more reduced fit the data best and chemically are the most reasonable. One such model designates Ni-SI as nickel(2+) dithiolate, Ni-C as nickel(1+) dithiol, and Ni-R as nickel(2+) dithiol hydride. This model can be used to rationalize the established properties of the Ni center and, in conjunction with the microstate concept, to reformulate a popular mechanism of catalysis into a tricyclic form. The only essential difference among the three interrelated catalytic cycles is the average oxidation state of the Fe−S clusters, not the states of the Ni center. Our analysis indicates that only the cycle operating with the Fe−S clusters predominantly in their reduced forms is reversible (able to reduce protons to H_2, as well as to oxidize H_2 to H^+). We propose that Ni-R reduces protons to H_2 only if its neighboring Fe−S cluster is reduced.

ACKNOWLEDGMENT

We thank Julie Kovacs, Marcetta Darensbourg, and William McMullen for helpful discussions.

APPENDIX

Simulation Procedure. Equilibrium constants for eqs 1−6 were obtained from the relation $K_i = \exp(\Delta EnF/RT)$, where $n = 2$ and $\Delta E = (E_{m(thionin)}' - E_{mi}')$. $E_{m(thionin)}' = +0.064$ V, and E_{mi}' is the midpoint potential for a generic site i. The total amount of oxidant added during the titration, in equivalents/mole, was divided into 50 points, and simulations were performed at each point. Using a program written in ASYST (Keithley Metrabyte), equilibrium concentrations of all redox species were determined at each point as follows. In the first step of a two-step process, each redox center was allowed to react, according to eqs 1−6, with one-sixth of the total amount of oxidant available at that point. Each center was then allowed to react with one-sixth of whatever oxidant remained after the first set of reactions. This process was repeated until either all of the oxidant was consumed or a constant amount of unreacted oxidant remained from cycle to cycle.

In the next step, using the concentrations obtained, each redox center was allowed to oxidize or reduce every other redox center in Hase according to the 15 equilibrium expressions given in eqs 28−42:

$$\text{Ni-R} + [Fe_{4b}]^{2+} \rightleftharpoons \text{Ni-C} + [Fe_{4b}]^{1+} \quad (28)$$

$$[Fe_{4a}]^{1+} + [Fe_{4b}]^{2+} \rightleftharpoons [Fe_{4a}]^{2+} + [Fe_{4b}]^{1+} \quad (29)$$

$$\text{Ni-C} + [Fe_{4b}]^{2+} \rightleftharpoons \text{Ni-SI} + [Fe_{4b}]^{1+} + H^+ \quad (30)$$

$$\text{Ni-SI} + [Fe_{4b}]^{2+} \rightleftharpoons \text{Ni-B} + [Fe_{4b}]^{1+} \quad (31)$$

$$[Fe_3]^{0} + [Fe_{4b}]^{2+} \rightleftharpoons [Fe_3]^{1+} + [Fe_{4b}]^{1+} \quad (32)$$

$$\text{Ni-C} + [Fe_{4a}]^{1+} \rightleftharpoons \text{Ni-R} + [Fe_{4a}]^{2+} \quad (33)$$

$$\text{Ni-C} + [Fe_3]^{0} \rightleftharpoons \text{Ni-R} + [Fe_3]^{1+} \quad (34)$$

$$\text{Ni-C} + [Fe_{4a}]^{2+} \rightleftharpoons \text{Ni-SI} + [Fe_{4a}]^{1+} + H^+ \quad (35)$$

$$\text{Ni-SI} + [Fe_{4a}]^{2+} \rightleftharpoons \text{Ni-B} + [Fe_{4a}]^{1+} \quad (36)$$

$$[Fe_3]^{0} + [Fe_{4a}]^{2+} \rightleftharpoons [Fe_3]^{1+} + [Fe_{4a}]^{1+} \quad (37)$$

$$\text{Ni-SI} + [Fe_3]^{0} + H^+ \rightleftharpoons \text{Ni-C} + [Fe_3]^{1+} \quad (38)$$

$$\text{Ni-B} + [Fe_3]^{0} \rightleftharpoons \text{Ni-SI} + [Fe_3]^{1+} \quad (39)$$

$$\text{Ni-C} + \text{Ni-SI} \rightleftharpoons \text{Ni-R} + \text{Ni-B} \quad (40)$$

$$\text{Ni-C} + \text{Ni-B} \rightleftharpoons 2\text{Ni-SI} + H^+ \quad (41)$$

$$\text{Ni-SI} + \text{Ni-R} + H^+ \rightleftharpoons 2\text{Ni-C} \quad (42)$$

These expressions were each solved using the concentrations obtained from the first step. The averages of the resulting concentrations were used as the initial concentrations for a subsequent cycle of these 15 expressions. This cycling was repeated until equilibrium concentrations for all redox centers were established simultaneously, checked by comparing the concentration ratios defining the equilibrium constants to the equilibrium constants assumed for that simulation.

Assessing the Quality of the Fits. Line segments connecting the data points of Figure 1 were constructed, with 50 segment points (X_{seg}, Y_{seg}) inserted between each EPR data point and 7 segment points between each absorbance data point. The number of points in all of the segmented titration curves was designated N. The normalized distance, D_{seg}, between each segment point and any of the 50

simulation points (X_{sim}, Y_{sim}) was determined according to

$$D_{seg} = [[(X_{seg} - X_{sim})/(X_{max} - X_{min})]^2 + [(Y_{seg} - Y_{sim})/(Y_{max} - Y_{min})]^2]^{1/2} \quad (43)$$

$(X_{max} - X_{min})$ is the length of the abscissa and $(Y_{max} - Y_{min})$ is the length of the ordinate. There were 50 D_{seg} values for each segment point, and that with the smallest value was designated D_{segmin}. There were N D_{segmin} values overall, one for each segment point.

Fits of simulated Ni-C titration curves to the experimental Ni-C curves were evaluated by the quality-of-fit parameter, $Q_{Ni\text{-}C}$, defined by

$$Q_{Ni\text{-}C} = \frac{1}{N_{segmin=1}} \sum^{N} D_{segmin} \quad (44)$$

The fits of the simulated titration curves to the experimental Ni-B, $g = 2.02$, A_{410}, and A_{600} titration curves were evaluated similarly using the quality-of-fit parameters $Q_{Ni\text{-}B}$, $Q_{2.02}$, Q_{410}, and Q_{600}, defined similarly. The overall quality-of-fit parameter for each of the four titrations (Q_{fit}) was defined by

$$Q_{fit} = Q_{Ni\text{-}C} + Q_{Ni\text{-}B} + Q_{2.02} + Q_{410} + Q_{600} \quad (45)$$

Three types of parameters, including (i) E_m' for each redox reaction, (ii) the enzyme concentration, $[Hase]_{sim}$, and (iii) the number of equivalents/mole that the sample was oxidized at the beginning of the titration, were varied to achieve the lowest Q_{fit} to each titration (called $Q_{best\text{-}fit}$). For each titration, the lowest $Q_{best\text{-}fit}$ obtained using any of the three models was called Q_{min}. The relative fidelity of the models in simulating the shapes of the titration curves was evaluated by the $Q_{best\text{-}fit}/Q_{min}$ ratio.

Calculating Chemical Potentials. In principle, the chemical potential E for each point of the titration could be calculated using the Nernst equation, the best-fit E_m', and the concentrations of the oxidized and reduced forms of any of the redox species (i) in Hase. In practice, the reliability of the calculated E_i (the E obtained using species i) depended on the concentrations of the oxidized and reduced forms of i and on the oxidized/reduced ratio for i. E_i values were considered reliable when the concentrations of i_{ox}/i_{tot} and i_{red}/i_{tot} were >0.000 01, and when i_{ox}/i_{red} was between 80:1 and 1:80. At each simulation point, E_i values were calculated for each redox species that fulfilled these criteria, and the average was taken as E for that point.

SUPPLEMENTARY MATERIAL AVAILABLE

Table of best-fit parameters according to FED models, figures showing the simulation of titrations 2−4 according to TED, and figures showing the simulation of titrations 2−4 according to FED (7 pages). Ordering information is given on any current masthead page.

REFERENCES

Bagyinka, C., Whitehead, J. P., & Maroney, M. J. (1993) *J. Am. Chem. Soc. 115*, 3576.

Baidya, N., Olmstead, M. M., Whitehead, J. P., Bagyinka, C., Maroney, M. J., & Mascharak, P. K. (1992a) *Inorg. Chem. 31*, 3612.

Baidya, N., Olmstead, M. M., & Mascharak, P. K. (1992b) *J. Am. Chem. Soc. 114*, 9666.

Barondeau, D. P., Roberts, L. M., & Lindahl, P. A. (1994) *J. Am. Chem. Soc. 116*, 3442.

Bowmaker, G. A., Boyd, P. D. W., Campbell, G. K., Hope, J. M., & Martin, R. L. (1982) *Inorg. Chem. 21*, 1152.

Cammack, R., Patil, D. S., Hatchikian, E. C., & Fernandez, V. M. (1987) *Biochim. Biophys. Acta 912*, 98.

Cammack, R., Fernandez, V. M., & Schneider, K. (1988) in *The Bioinorganic Chemistry of Nickel* (Lancaster, J., Ed.) Chapter 8, VCH Publishers, New York.

Crabtree, R. H. (1986) *Inorg. Chim. Acta 125*, L7.

DerVartanian, D. V., Kruger, H. J., Peck, H. D., Jr., & LeGall, J. (1985) *Rev. Port. Quim. 27*, 70.

Eidsness, M. K., Sullivan, R. J., & Scott, R. A. (1988) In *The Bioinorganic Chemistry of Nickel* (Lancaster, J., Ed.) Chapter 4, VCH Publishers, New York.

Fan, C., Teixeira, M., Moura, J. J. G., Moura, I., Huynh, B. H., LeGall, J., Peck, H. D., & Hoffman, B. M. (1991) *J. Am. Chem. Soc. 113*, 20.

Farmer, P. J., Reibenspies, J. H., Lindahl, P. A., & Darensbourg, M. Y. (1993) *J. Am. Chem. Soc. 115*, 4665.

Fernandez, V. M., Hatchikian, E. C., & Cammack, R. (1985) *Biochim. Biophys. Acta 832*, 69.

Geoffroy, G. L., & Wrighton, M. S. (1979) *Organometallic Photochemistry*, Chapter 7, Academic Press, New York.

Gore, E. S., & Busch, D. H. (1973) *Inorg. Chem. 12*, 1.

Hallahan, D. L., Fernandez, V. M., Hatchikian, E. C., & Cammack, R. (1986) *Biochim. Biophys. Acta 874*, 72.

Huang, Y. H., Park, J. B., Adams, M. W. W., & Johnson, M. K. (1993) *Inorg. Chem. 32*, 375.

Kojima, N., Fox, J. A., Hausinger, R. P., Daniels, L., Orme-Johnson, W. H., & Walsh, C. (1983) *Proc. Natl. Acad. Sci. U.S.A. 80*, 378.

Kovacs, J. (1993) in *Advances in Inorganic Biochemistry* (Eichhorn, G. L., & Marzilli, L. G., Eds.) Vol. 9, Chapter 5, Prentice-Hall, Englewood Cliffs, NJ.

Krasna, A. I., & Rittenberg, D. (1954) *J. Am. Chem. Soc. 76*, 3015.

Kristjansdottir, S. S., Norton, J. R. (1992) *Transition Metal Hydrides*, Chapter 9, VCH Publishers, New York.

Krüger, H. J., & Holm, R. H. (1987) *Inorg. Chem. 26*, 3645.

Krüger, H. J., & Holm, R. H. (1990) *J. Am. Chem. Soc. 112*, 2955.

Lewis, J., & Schröder, M. (1982) *J. Chem. Soc., Dalton Trans.* 1085.

Lovecchio, F. V., Gore, E. S., & Busch, D. H. (1974) *J. Am. Chem. Soc. 96*, 3109.

Moura, J. J. G., Teixeira, M., Moura, I., & LeGall, J. (1988) in *The Bioinorganic Chemistry of Nickel* (Lancaster, J., Ed.) Chapter 9, VCH Publishers, New York.

Palmer, G., & Olson, J. S. (1980) in *Molybdenum and Molybdenum-Containing Enzymes* (Coughlan, M. P., Ed.) Chapter 5, Pergamon Press, New York.

Prince, R. C., & Adams, M. W. W. (1987) *J. Biol. Chem. 262*, 5128.

Saint-Joly, C., Mari, A., Gleizes, A., Dartiguenave, M., Dartiguenave, Y., & Galy, J. (1980) *Inorg. Chem. 19*, 2403.

Salerno, J. C. (1988) in *The Bioinorganic Chemistry of Nickel* (Lancaster, J., Ed.) Chapter 3, VCH Publishers, New York.

Shin, W., & Lindahl, P. A. (1992) *Biochemistry 31*, 12870.

Shoner, S. C., Olmstead, M. M., & Kovacs, J. A. (1994) *Inorg. Chem. 33*, 7.

Teixeira, M., Moura, I., Xavier, A. V., DerVartanian, D. V., LeGall, J., Peck, H. D., Huynh, B. H., & Moura, J. J. G. (1983) *Eur. J. Biochem. 130*, 481.

Teixeira, M., Moura, I., Xavier, A. V., Huynh, B. H., DerVartanian, D. V., Peck, H. D., LeGall, J., & Moura, J. J. G. (1985) *J. Biol. Chem. 260*, 8942.

Teixeira, M., Moura, I., Xavier, A. V., Moura, J. J. G., LeGall, J., DerVartanian, D. V., Peck, H. D., & Huynh, B. H. (1989) *J. Biol. Chem. 264*, 16435.

Van der Zwaan, J. W., Albracht, S. P. J., Fontijn, R. D., & Slater, E. C. (1985) *FEBS Lett. 179*, 271.

Van der Zwaan, J. W., Albracht, S. P. J., Fontijn, R. D., & Roelofs, Y. B. M. (1986) *Biochim. Biophys. Acta 872*, 208.

Van der Zwaan, J. W., Coremans, J. M. C. C., Bouwens, E. C. M., & Albracht, S. P. J. (1987) *Eur. J. Biochem. 169*, 377.

Van der Zwaan, J. W., Coremans, J. M. C. C., Bouwens, E. C. M., & Albracht, S. P. J. (1990) *Biochim. Biophys. Acta 1041*, 101.

Voordouw, G. (1992) *Adv. Inorg. Chem. 38*, 397.

Whitehead, J. P., Gurbiel, R. J., Bagyinka, C., Hoffman, B. M., & Maroney, M. J. (1993) *J. Am. Chem. Soc. 115*, 5629.